NON-STANDARD GRIDS

R J Purser
National Centers for Environmental Prediction
Washington D.C., U.S.A

Abstract: The recent trend in computer architecture towards massively parallel systems has been partly responsible for stimulating renewed interest in non-standard configurations for the computational grids used in global numerical weather prediction. We examine some of the alternatives here, together with their potential advantages and their possible drawbacks.

1. INTRODUCTION

The evident trend in super-computer architectures towards massively parallel configurations of processors has revived interest in the use of grid point frameworks, as alternatives to spectral methods, for global forecast and climate models. Grid point models seem to lend themselves more easily to "domain decomposition" – a division of labour among processors based upon some geographical partitioning of the computational load. "Standard" grids, by which we mean locally quadrilateral horizontal grids aligned everywhere with the latitude and longitude coordinate system, are not necessarily the best frameworks to use; the meridians crowd towards the poles (fig. 1a) necessitating either excessively short time steps or frequent application of special filters to preserve linear numerical stability, and the strong polar singularities themselves must be treated separately. It is possible to alleviate these difficulties, following Gates and Riegel 1962, Kurihara 1965, by adopting a "reduced" grid, as shown in fig. 1b, or a "skipped" grid, as illustrated in fig. 1c. Such solutions preserve approximately constant spatial resolution zonally at all latitudes, but only at the additional computational cost and inconvenience associated with the zonal interpolations now needed to "fill the gaps" pole-ward of each transitional latitude where the grid's zonal resolution is made to change abruptly.

An alternative is to employ a "non-standard" grid, which can mean either quadrilateral or triangular/hexagonal elements locally, and which conforms globally to coordinates other than latitude and longitude (or a trivial rotation of this system). While not attempting a comprehensive review, we here describe some old and new investigations into the use of alternative, polyhedral, grid frameworks, none of which are without their own special problems. Section 2 describes some of the more promising grid topologies that allow mapping to the surface of the sphere. Section 3 presents some of the systematic construction techniques for generating these map transformations. It also discusses ways in which the metrical characteristics of the grid may be chosen, and perhaps optimised, to ensure good numerical behaviour and computational efficiency. The triangular/hexagonal grids, with locally six-fold rotational symmetry and with three (instead of two) locally intersecting families of horizontal grid lines, present their own challenges to the numerical analyst, quite apart from those associated with their global topologies. Section 4 discusses some local numerical considerations pertaining to

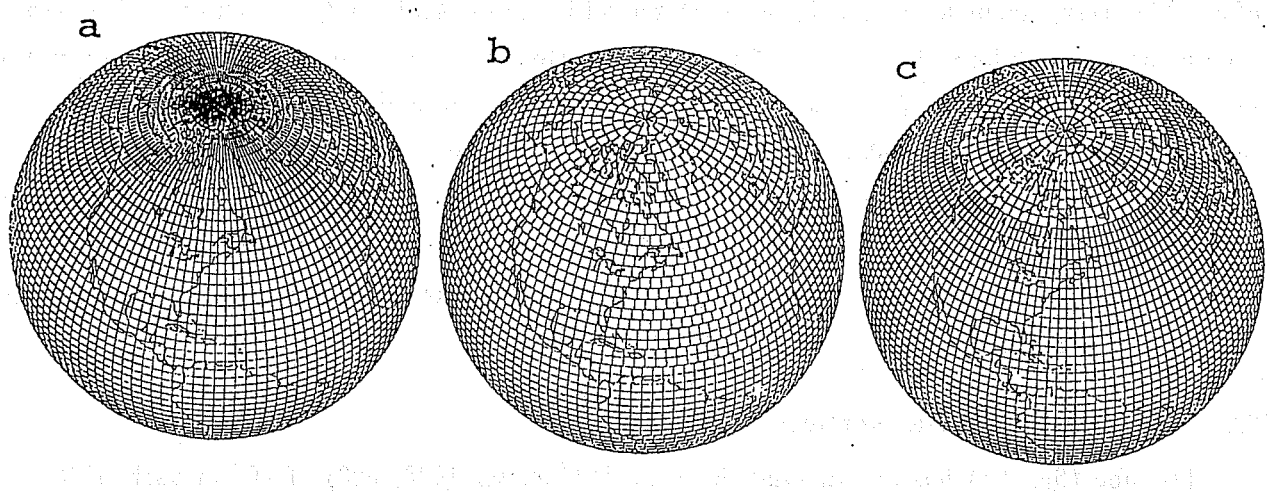

Figure 1. Comparison of latitude – longitude grids: (a) unmodified; (b) reduced; (c) skipped.

both staggered and unstaggered versions of these grids, which, for brevity, we shall subsequently refer to merely as "triangular". Finally, we summarize the apparent advantages and disadvantages of the possible choices of non-standard grids discussed.

2. GLOBAL GRIDS BASED ON POLYHEDRA

Since the surface of a convex polyhedon, such as a cube, shares the same topology as the surface of the sphere, then, if the surface of the polyhedron admits a natural gridding, that gridding can be mapped continuously onto the sphere. For a regular polyhedron with triangular faces, such as the twenty-sided regular icosahedron, the natural gridding uses a triangular grid aligned with the twenty "large triangles". For a cube, the most natural surface gridding uses a square grid aligned with the edges of the cube. Various alternative grid orientations are also possible. A square grid may be oriented at 45° to the edges of the cube in which it is inscribed, or a triangular grid may be oriented at 30° to the edges of its parent icosahedron; both cases preserve the original polyhedron's symmetries. There are other oblique grid orientations which break the symmetry by introducing an artificial "chirality" or "handedness" to the grid configuration but, to this author's knowledge, these options have never found uses in numerical models.

2.1 Early applications.

Both the icosahedral and cubic grids have been used, from time to time, in global numerical models of the atmosphere. Sadourny et al. (1968) performed experiments using an icosahedral grid as the basis of a barotropic vorticity model. Williamson (1968, 1970) independently introduced this grid arrangement in studies applied to finite difference representations of the barotropic vorticity and barotropic primitive equations, while Cullen (1974) showed how to use the icosahedral framework for integrations of the primitive equations using finite element methods. Masuda and Ohnishi (1987)

devised an integration scheme for the primitive equations on the icosahedral grid that used stream-function and velocity potential as two of the primitive variables. Sadourny (1972) pioneered the use of a cubic arrangement for a global grid point model based on Arakawa-type energy- and enstrophy-conserving finite differencing. Most of these early attempts to use nonstandard grid encountered numerical artifacts arising from the intrusion of the grid's own symmetries into components of the computed solutions. The simplest mappings to the sphere do not preserve continuity of the derivatives of the metric terms on passage from one face of the associated solid to its neighbour. We shall see below that this defect, at least, can be remedied. A more intractable problem is the continued presence of a coordinate singularity, albeit a weak one, at each vertex. The nature of these singularities deserves some discussion.

2.2 Grid distortion near vertices.

The cube (fig. 2a) has an "angular deficiency" (Coxeter 1973, p23) of 90° at each of its eight vertices where the corners of only three panels come together, forcing 270° of "map space" angle to span the full 360° azimuth at the corresponding geographical point . The same angular deficiency per vertex is also obtained in the case of the double-sided octagon, or octagonal "dihedron" (Coxeter 1973) which, at least for mapping purposes, belongs within the class of polyhedra also (fig. 2b).

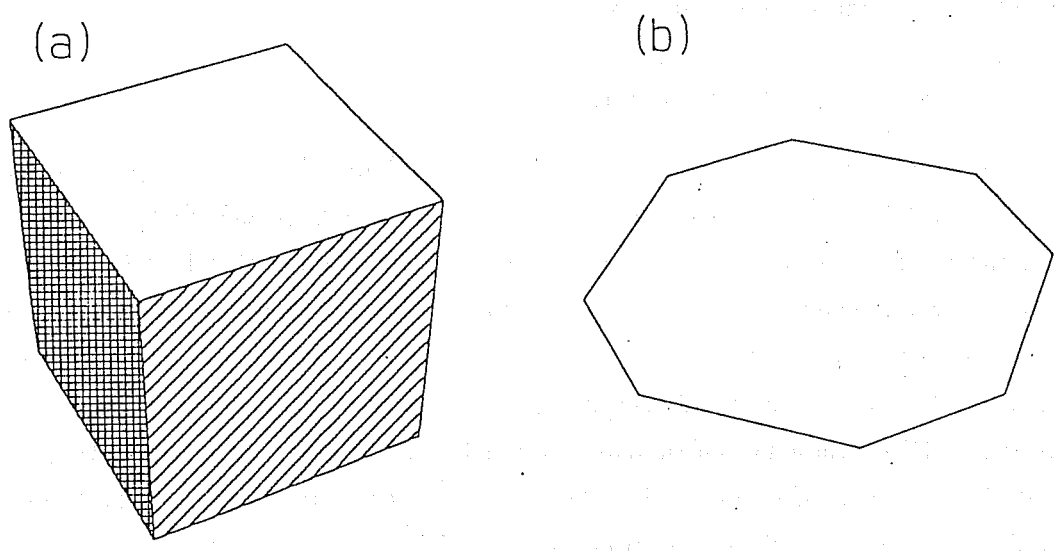

Figure 2. Polyhedra admitting a square-gridding of their surfaces: (a) the cube; (b) an octagonal dihedron.

The icosahedron, depicted in fig. 3a, has an angular deficiency of 60° at each of its twelve vertices, where the 60° corners of five triangular panels come together.

We can take the angular deficiency as an effective measure of the unavoidable grid distortion surrounding the vertex. This distortion might be spread continuously across all azimuth angles in the case of a grid constructed to be smooth across the polyhedron's edges, in which case, we find that at least one of the family of grid coordinates suffers unbounded curvature in the neighbourhood of the vertex. Alternatively, we can choose to maintain separate well-behaved grid coordinates on separate faces of the polyhedron and concentrate all the difficulties in the form of coordinate discontinuities

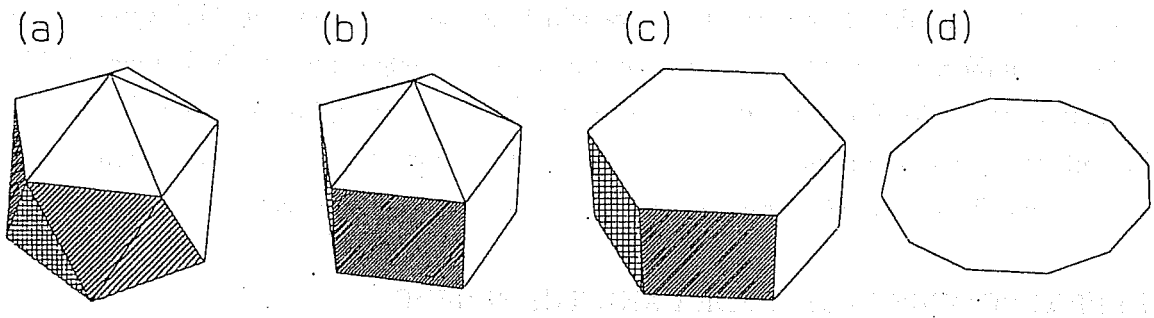

Figure 3. Polyhedra admitting a triangular-gridding of their surfaces: (a) the icosahedron; (b) the twisted icosahedron; (c) the hexagonal prism; (d) a dodecagonal dihedron.

confined to the radiating edges. The total angular deficiency of any simply connected polyhedron sums to 720° (equivalently, the areal density of angular deficiency, known as the "Gaussian curvature", integrates to 4π radians over the surface of any simply connected solid). It is therefore unfortunate that the regular solid with the greatest number of vertices (and therefore the most benign singularities) — the (twelve-sided) dodecahedron, possessing twenty vertices but pentagonal faces, is also distinguished as being the *only* one of the five so-called "platonic solids" that does *not* admit a natural gridding of its surface! It is partly owing to the fact that the icosahedron is the next best choice, with twelve vertices, that this form has been so often considered as the framework for global models. However, the icosahedron also possesses the virtue of a very high order of symmetry (the order of the group of proper and inverting rigid rotations of the icosahedron is 120, as compared to 48 for the cube). It is this high degree of symmetry which enables the icosahedral grid resolution to be kept very homogeneous while the moderately large number of its vertices ensures that the grid distortion about each one is relatively small.

2.3 Choices based on symmetries.

There are aspects to the symmetry properties of the icosahedron that are undesirable; when oriented with a vertex at each pole in order to maximise the degree of zonal symmetry (five-fold), the inscribed grid fails to exhibit mirror-symmetry about the equatorial plane. A spurious wave-five pattern, with opposite phases in the two hemispheres, is one way in which the grid's symmetry can intrude on the simulated flow over the course of a long integration (Masudo and Ohnishi 1987). In a modification of the icosahedral arrangement, which they refer to as the "twisted icosahedral" grid, Heikes and Randall (1995a, 1995b) effectively turn one hemisphere's configuration of vertices by 36° with respect to the other hemisphere's. Then the triangular grid is able to link up the vertices almost as before, except now with mirror symmetry across the equator. A remaining asymmetry, that two

vertices are distinguished by being at the poles while the other ten, in rings of five, at a symmetrical pair of middle latitudes, can be removed by adopting a grid with six-fold zonal symmetry. The twisted icosahedral grid corresponds to the surface gridding of a polyhedron formed by appending pentagonal pyramids to both ends of a pentagonal prism, the result of which is depicted in fig. 3b; the associated polyhedron of the grid with six-fold zonal symmetry is simply a hexagonal prism, shown in fig. 3c. Fig. 3d shows one of the possible dodecagonal dihedra which, for certain ratios for the lengths of alternate edges, admits a uniform triangular gridding continuous across edges just as the octagonal dihedron, for particular ratios of *its* alternate edges, allows a uniform square gridding continuous across edges. To an extent, the numerical performance, of any of these polyhedron-based grids is dependent upon the manner in which the mapping from polyhedron to sphere is accomplished.

3. MAPPING BETWEEN POLYHEDRA AND THE SPHERE

Arguably, the simplest of all mappings between the uniformly gridded surface of a convex polyhedron and the surface of the sphere is that obtained by central projection — a "gnomonic" projection, in the terminology of cartography. However, despite its simplicity, this method has *not* found much favour amongst modelers, presumably because it leads to a less homogeneous distribution of grid points than can be obtained using other map projections.

3.1 Quasi-homogeneous grids.

For the icosahedral grid, Sadourny et al. (1968) placed two of the vertices at the poles so that each one of the 20 congruent large triangles, with great circle arcs for sides, had one of these sides oriented east–west. The other pair of sides were subdivided into N intervals of equal geographical distance, with the corresponding pairs of the new points separating these intervals then joined by new great circle arcs to form all the grid lines running approximately zonally. The triangular grid was completed by arranging, for each one of these approximately zonal arcs, that the final grid points placed along them were also separated by equal great circle distances. In this way an almost homogeneous resolution was achieved. Williamson (1968) used a qualitatively similar geometrical procedure to achieve the same objective of almost homogeneous resolution for a triangular grid oriented at 30° with respect to the large triangles of the projected icosahedron. Cullen (1974) also placed vertices at each pole but made the sides of the large triangles straight lines in the space linear in latitude and longitude. He obtained satisfactory numerical results from a further triangular subdivision, also linear in latitude and longitude. This grid had the convenient property that one of the three families of grid lines in each large triangle were precisely lines of constant latitude.

The symmetry of the original icosahedron is formally broken by each of these grid constructions, but in the case of the cube, whose square grid is unencumbered by the restriction that *three* families of grid lines must always intersect at the grid points, Sadourny (1972) exhibited a gnomonic projection of a (nonuniformly spaced) rectangular gridding of the cube onto the sphere which gave a quasi-uniform resolution while preserving the original cubic symmetries. In the case of the twisted icosahedral grid of Heikes and Randall (1995a), the final grid is constructed via a process of recursive subdivision in

which, at each successive stage, the midpoints of the sides previous small spherical triangles are joined by arcs to form a new triangular grid of twice the resolution. This procedure obviously restricts the final grid dimensions to be a power of two refinement of the coarsest configuration of the same topology, but they had other reasons, related to the efficient implementation of multigrid solvers, for adopting this restriction in any case. Giraldo (1997) has used a similar method of successive refinement for the true icosahedron in his recent adaptation of the Lagrange-Galerkin method to the simulation of flow on the sphere.

The grid constructions above all exemplify the concentration of grid problems along the polyhedral edges, where there can be no smooth continuity from one polyhedral face to the next. It would appear that the constructions based on successive grid refinement also lead to a formal lack of smoothness in the interior of each large triangle, which would limit the applicability of generic high-order differencing schemes to such grids. Swarztrauber et al. (1997) have found a practical way of obtaining formally accurate differencing schemes on an icosahedral grid without assuming the usual conditions of grid regularity. Their method is based on a form of constrained least-squares optimisation of the coefficients of the template at each point of application. (In section 4.2 we give a more detailed outline of how to formulate a method, similar in spirit to this, that is needed to avoid ambiguity even in the evaluation of certain high-order differencing coefficients on a plane triangular grid.) Unless customised numerical schemes are employed at the polyhedral edges, where the metrics of the grids we have discussed become discontinuous, unacceptably large truncation errors can result. We therefore proceed to consider grid construction designed to address these edge defects.

3.2 Cubic grid, partially continuous across edges.

In one of the recent attempts to revive the cubic geometry for use on massively parallel processor (MPP) computers, Ronchi et al. (1995, 1996) find a partial remedy for the edge problems in the following way. They define three families of great circles, each family having a common axis (passing through the centres of an opposing pair of the large squares of the symmetrically projected cube). In each family, the planes defined by successive great circles differ in angle from one another by multiples of a constant fraction of a right-angle (so that the cube's edges each belong to one of these families). The grid spanning each face of the spherical cube is constucted using arcs from the two of the families of great circles which fan out from the axes piercing the centres of the neighbouring four large squares. Like the construction of Sadourny (1972), the resulting grid can be regarded as the gnomonic projection of some *nonuniform* rectangular gridding of the surface of the inscribed cube. But it has the crucial property that, passing across the edge of each large square, the coordinate which is changing transversally to this edge, remains smoothly continuous (except, possibly, for a trivial additive constant or sign change) with the corresponding coordinate used in the neighbouring large square. In this way, the necessary discontinuity across edges is confined to only *one* of the two horizontal coordinates and, even at one of the corners, no actual coordinate singularity is encountered.

As shown in fig 4., the construction of Ronchi et al. implies that, by extrapolating each large square's grid beyond the edge, it is possible to recover the values at the points of the extrapolated grid

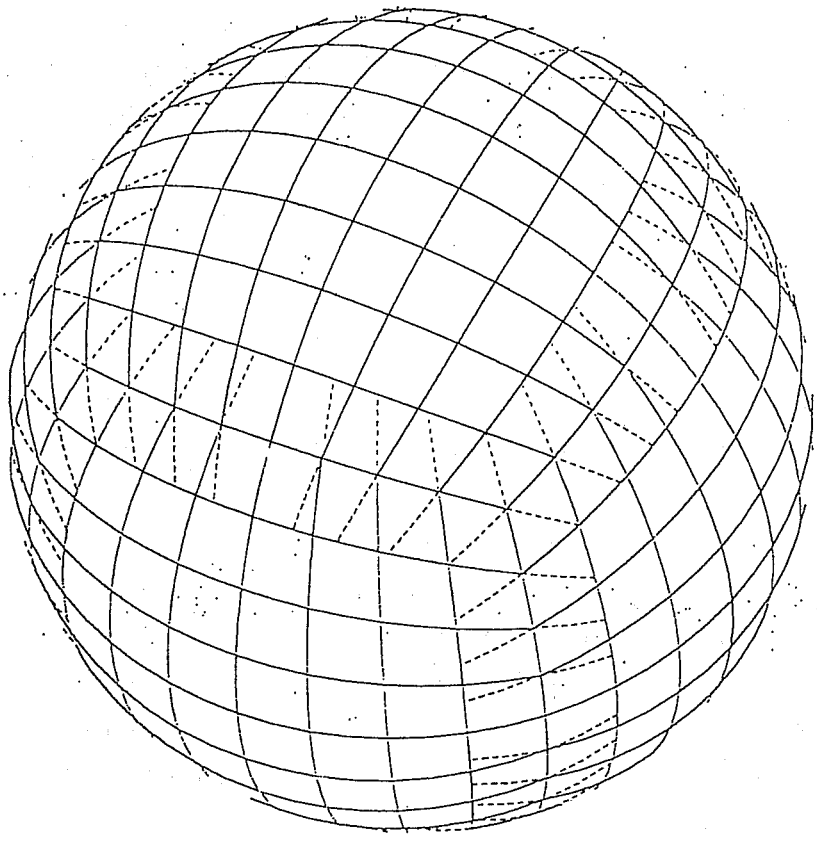

Figure 4. Schematic form of the cubic grid of Ronchi et al. (1996)

by only interpolating *one-dimensionally*, along each grid line common to the two adjoining square panels' coordinate frames. In this way, they are able to apply high-order differencing methods in an efficient manner and obtain extremely accurate numerical simulations of idealized fluid flows. The resolution of the grid is kept moderately consistent and the computations are readily distributed across multiple processors.

3.3 Conformal grids, fully continuous across edges.

Except for the discrete vertex singularities it is possible to find various mappings from a polyhedron to the sphere preserving smooth continuity (except at vertices, of course) of *all* grid coordinates from one face to the next. There is a sense in which the "smoothest" of such mappings is one which also preserves angles correctly; such a mapping is called "conformal" and the theory of two-dimensional surface mappings with this transitive property is intimately associated with the classical theory of complex analytic functions (e.g., Schwerdtfeger 1979). For a smooth surface of any compact simply-connected solid, the existence of a conformal mapping to the sphere (and, by transitivity, to any other simply-connected solid's surface) is assured; for a simply-connected polyhedron, whose Gaussian curvature is impulsively infinite only at the discrete vertices, there are mappings to the sphere that are conformal everywhere except at the vertices themselves. The transformations are not unique, however, since the sphere is conformally mapped to itself by members of the six-parameter continuous group of

"Möbius" transformations which consist, in addition to rigid rotations (three parameters), a differential scale-dilatation (one parameter) symmetrically centred about some axis (two parameters). Classically, these transformations appear in the context of analytic complex functions; the identification of points on the sphere with points in the complex plane being established through stereographic projection (which we discuss below). In the context of numerical weather prediction, these transformations are perhaps more familiar as the transformations of Schmidt (1977), who first realised that they offer a way to obtain enhanced regional detail in a global spectral model. They are applied quite successfully by Courtier and Geleyn (1988) for the ARPEGE operational forecasting system of Météo-France. We shall see below that these transformations have a role to play also in the design of some non-standard grids.

Each of the polyhedra illustrated in figs. 2 and 3 exhibit a symmetry between their upper and lower halves which, under conformal mapping to the sphere, can be preserved as a symmetry between the two hemispheres. Fixing the longitude then makes the conformal mapping unique. Rančić et al. (1996) investigated the use of the conformal cubic transformation as a framework for grid point modelling lending itself to application to MPPs, comparing it with variants of the gnomonic projection. It is instructive to examine the methods used to obtain this most symmetrical conformal cubic transformation since, with only minor adaptation, the same method can be applied to derive conformal transformations of a great variety of polyhedral surfaces, including the "improper" ones exemplified by the dihedra of figs. 2 and 3.

The problem of conformally transforming between a map point on the surface of the unit-sided cube and the corresponding target point of the sphere can be split into a sequence of separate steps. The first step identifies the map-point with a complex number, z, by rotating and (perhaps) reflecting the square face containing this point into the first quadrant (positive real and imaginary components) of the complex plane in such a way that the nearest vertex, V, to the point becomes the complex origin and the nearest edge becomes the segment $[0, 1]$ of the real axis. The aim of the next step is to find and apply the appropriate complex analytic function to this z whose result, w, will be the complex stereographic image of the target point for the stereographic mapping whose projection axis is identified with V (and the origins of the z and w-planes) and is scaled such that the centred unit-circle of the w-plane corresponds to the "equator" of this stereographic projection. This is an example of a projection in the optical sense, with rays intersecting at the point antipodal to the projection centre, as shown for this case in fig. 5. When we adopt the convention that the stereographic image of the positive real axis of z maps to the positive real axis of w, the particular complex function, $w(z)$, is unique and, by symmetry, applies (with appropriate re-orientation and identification of "nearest vertex" and "nearest edge") to *any* point on the sphere.

The angular deficiency at vertex V manifests itself as a "branch point" of the desired complex function, $w(z)$. In the general polyhedral case, an angular deficiency of α radians will imply,

$$w(z) = f\left(z^{2\pi/(2\pi-\alpha)}\right) \tag{3.1}$$

for some function f that remains analytic at $z = 0$. In the cubic case, w is therefore a locally analytic function of $z^{4/3}$, but we can also infer from the three-fold rotational symmetry of the cube around V

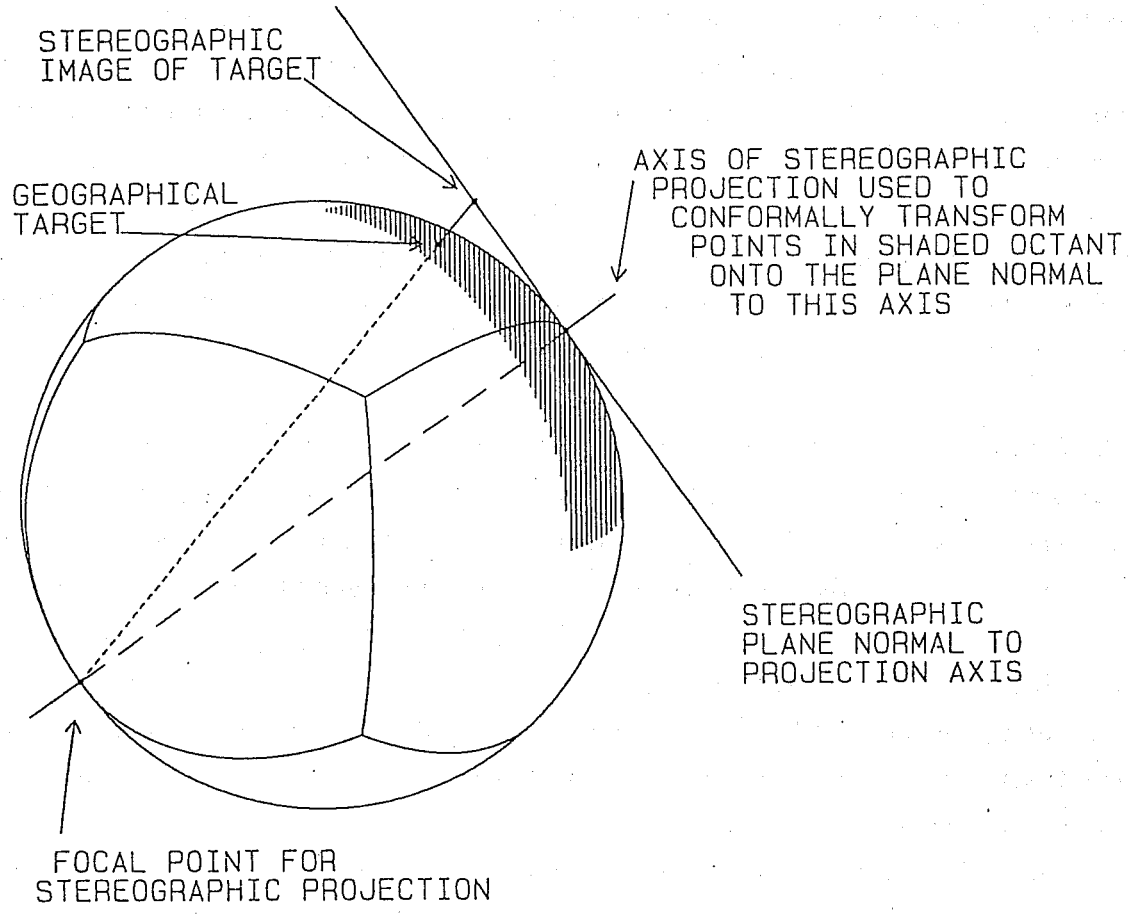

Figure 5. Optical projection used to construct the stereographic w-plane image of a target point on the sphere.

(see fig. 6) that, in the expansion of f, the coefficients of z^m vanish except when $\mathrm{mod}(m, 3) = 1$, and hence, the functional relationship is expanded more compactly in this case by,

$$w^3 = W(z^4) \equiv \sum_{k=1} A_k z^{4k}. \tag{3.2}$$

Moreover, since we have reflection symmetry about the edge that we have mapped to the real axes of z and w, it also follows that the Taylor coefficients A_k in this especially symmetric case are all real.

For a less symmetrical polyhedron than the cube, a different function f belongs to each vertex and a separate set of coefficients must be dealt with at each vertex, together with possible auxiliary expansions (not involving a fractional-power term) at intermediate non-vertex points in order to ensure sufficient mutual overlaps of the discs of convergence. The overlaps are necessary because the coefficients themselves are deduced through the requirement of complete mutual self-consistency of all of these power-series expansions, which can only be verified (or corrected) when the entire circle of convergence of one expansion is covered by the discs of convergence of others. The radius of the disc of convergence of the Taylor series of an analytic complex function is the distance between the expansion centre and the nearest singularity of that function. In the case of the cubic mapping, the nearest singularities in the z domain are the locations which correspond to the three next-nearest vertices, implying a radius of unity in our example. Approximations to the set of the first few coefficients,

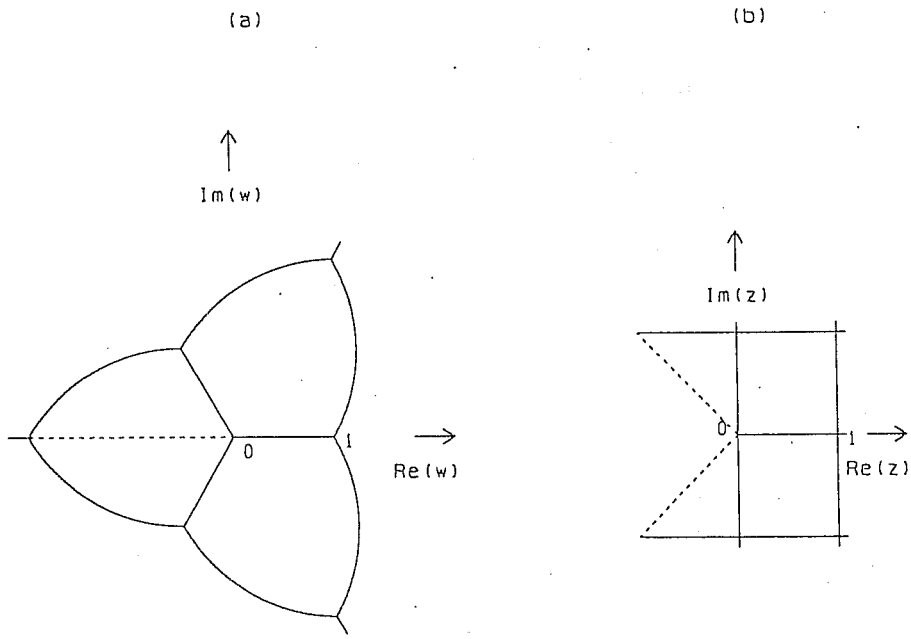

Figure 6. Configuration of the three faces of the cube in the neighbourhood of vertex V to: (a) the stereographic w-plane; (b) the rotated map plane, z.

A_k, can be improved iteratively by using the present estimates at each stage to evaluate the implied mapping function $W(z^4)$ along a circle very slightly smaller than the unit circle (to avoid direct contact with the singularities) based on the above power-series expansions pertaining to the neighbouring vertices. In the cubic case, we can obviously invoke the built-in symmetry. As described in detail in Rančić et al. (1996), the stereographic mapping relative to one vertex is readily transformed to the equivalent representation with respect to the stereographic mapping of another vertex of the cube. Let the radius of the verifying z-plane circle be $r < 1$ and express the location of a generic point there by $z = r\, e^{i\theta/4}$. W induces a complex periodic function, $g(\theta)$, for $\theta \in [-\pi, \pi]$ by,

$$g(\theta) = W(r^4\, e^{i\theta}). \tag{3.3}$$

But, by Fourier transformation,

$$g(\theta) = \sum_k \tilde{g}_k e^{ik\theta}, \tag{3.4}$$

and application of the Taylor series definition of W, we obtain the identity,

$$A_k = \tilde{g}_k / r^{4k}, \tag{3.5}$$

by which a new set of estimates for the A_k can be deduced. By uniformly spacing a suitable number of the sample points, $z = r\, e^{i\theta/4}$, over one period of θ (one quadrant of the circle in the z-plane shown in fig. 7), the fast Fourier transform method can be used to recover the new $\tilde{g}$ at each iteration. For the conformal cube, convergence of this procedure is rapid and the procedure need only be done once, and the generated coefficients stored for posterity. The first 30 coefficients A_k, together with the Taylor coefficients B_k for the inverse function, are given in Rančić et al. (1996). For other polyhedra, such as the octagonal dihedron, where more than one distinct series may be involved, numerical convergence of the coefficient-finding procedure is often assisted by a cautious "under-relaxation" of the increments

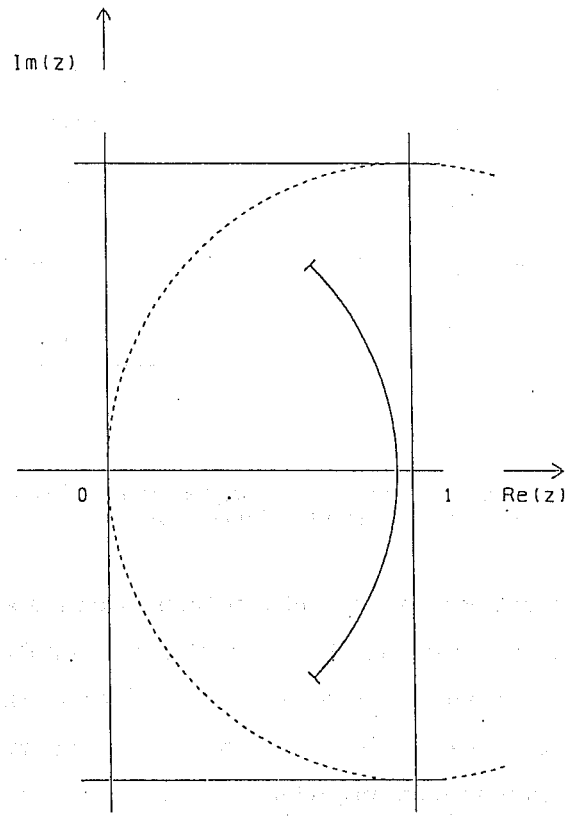

Figure 7. Schematic illustration of the arc (solid), just within the circle of convergence of the expansion about $z = 0$. on which the function $g(\theta)$ is evaluated during iterative refinement of the expansion coefficients for the conformal cubic mapping. The dashed arc shows the circle of convergence of the expansion about the vertex situated at $z = 1$.

implied at each stage, but in any case, the requisite self-consistency is ultimately achieved by some appropriate adaptation of the iterative method sketched here.

3.4 Quasi-homogeneous continuous grids.

The conformal mapping method gives us a grid that is smooth and continuous across the transformed edges of the associated polyhedron, even in the case in which the polyhedron is one of the degenerate double-sided polygons. For the icosahedron, whose conformal mapping is shown in fig. 8, we see that a reasonably homogeneous distribution of grid points is obtained and the singularity at each vertex is, at least to the eye, a very weak one. The minor remnant of spatial inhomogeneity is betrayed by the slight tendency for the grid points to cluster near the vertices. In the case of the cube, this tendency is intensified, as we see in fig. 9a. Fig. 9b shows the result of the application of a more general method of smooth grid generation, based on the solution of a variational principle designed to balance smoothness on the one hand with the goal of achieving spatial homogeneity on the other. Thompson et al. (1985) discuss a great variety of systematic techniques for the generation of computational grids with desirable properties, and many of the techniques they discuss involve variational methods. In the case of the grid shown in fig. 9b, the variational method is that suggested by Purser

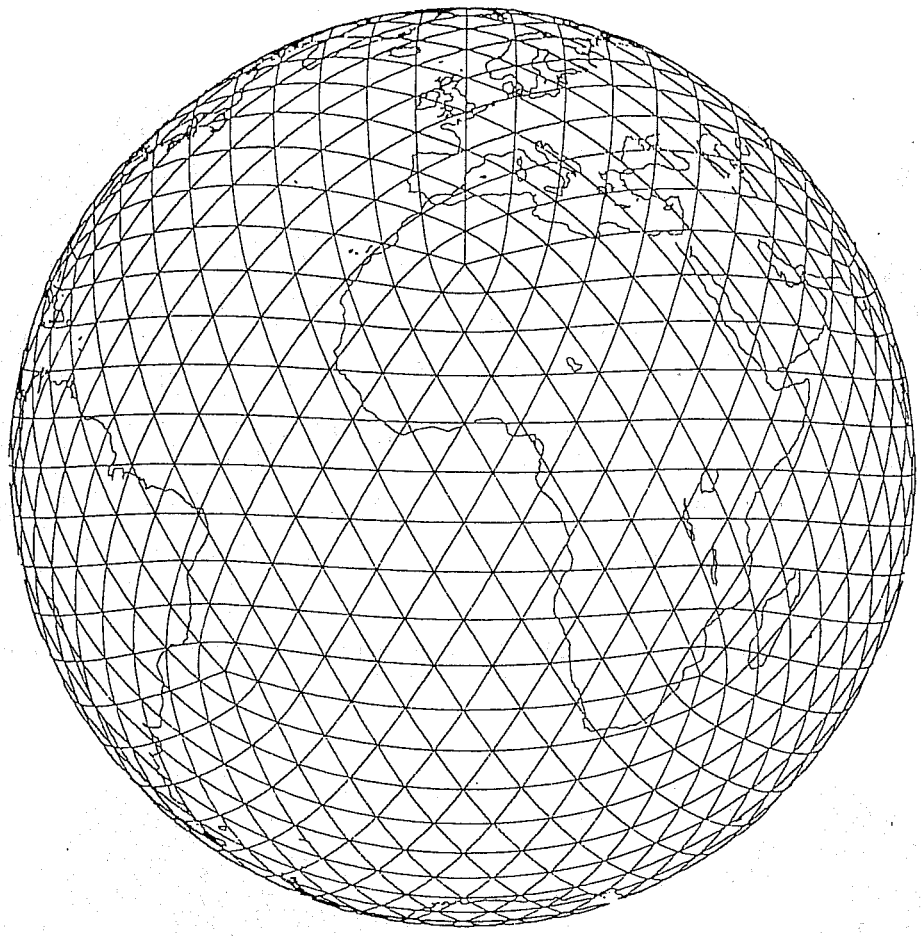

Figure 8. Conformal icosahedron grid.

and Rančić (1998), which can be stated as the extremisation of $\mathcal{L}(\mathbf{X}, \Lambda)$ defined by,

$$\mathcal{L} = \frac{1}{2} \int \int \left[\left| \frac{\partial \mathbf{X}}{\partial x} \right|^2 + \left| \frac{\partial \mathbf{X}}{\partial y} \right|^2 + a \ |\mathbf{Q} \cdot \mathbf{X}|^2 + \Lambda(|\mathbf{X}|^2 - 1) \right] dx \, dy. \tag{3.6}$$

where x and y are the two horizontal orthogonal map coordinates, $\mathbf{X}$ is the earth-centered cartesian 3-vector of the geographical point, taking the earth as a unit sphere, and

$$\mathbf{Q} = \frac{\partial \mathbf{X}}{\partial x} \times \frac{\partial \mathbf{X}}{\partial y}. \tag{3.7}$$

The constant, a, is a coefficient that determines the strength of the penalisation of spatial inhomogeneity; a large a implies that the quadrilateral elements of the grid are all almost the same areal size, while a small a causes the solution to revert towards the conformal mapping solution. The value of $a = 10$ was used to obtain fig. 9b. The scalar field, $\Lambda(x, y)$ is the Lagrange multiplier used to confine the vectors $\mathbf{X}$ of the solution to the unit sphere. The nonlinear Euler-Lagrange elliptic equations implied by the solution of our variational principle are,

$$\frac{\partial^2 \mathbf{X}}{\partial x^2} + \frac{\partial^2 \mathbf{X}}{\partial y^2} - a \left(\frac{\partial \mathbf{X}}{\partial x} \times \frac{\partial \mathbf{Q}}{\partial y} - \frac{\partial \mathbf{X}}{\partial y} \times \frac{\partial \mathbf{Q}}{\partial x} \right) = \Lambda \mathbf{X}, \tag{3.8}$$

$$|\mathbf{X}|^2 = 1. \tag{3.9}$$

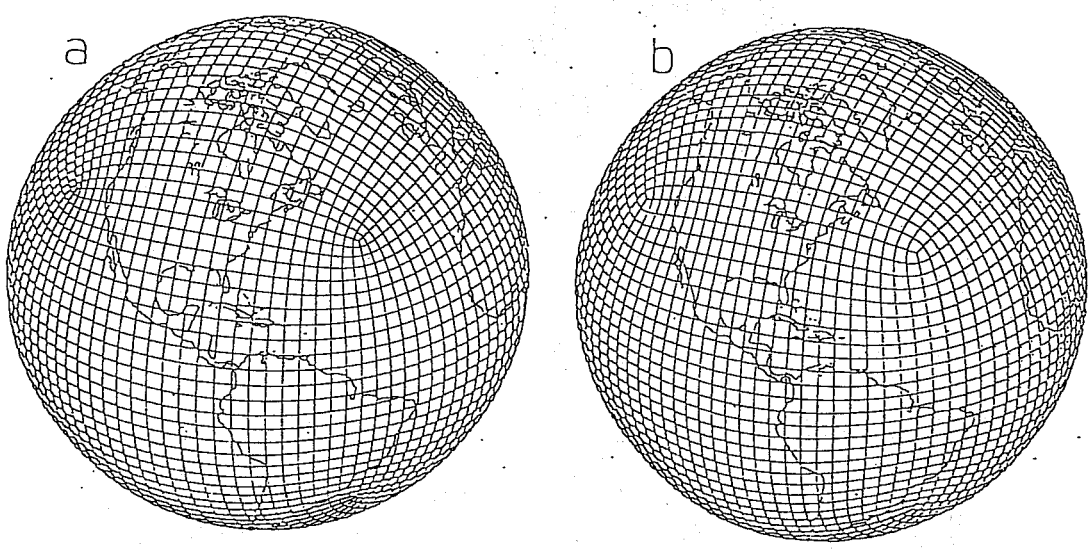

Figure 9. Smooth spherical cubic grids generated by: (a) conformal mapping; (b) quasi-homogeneous variational grid generation with parameter $a = 10$.

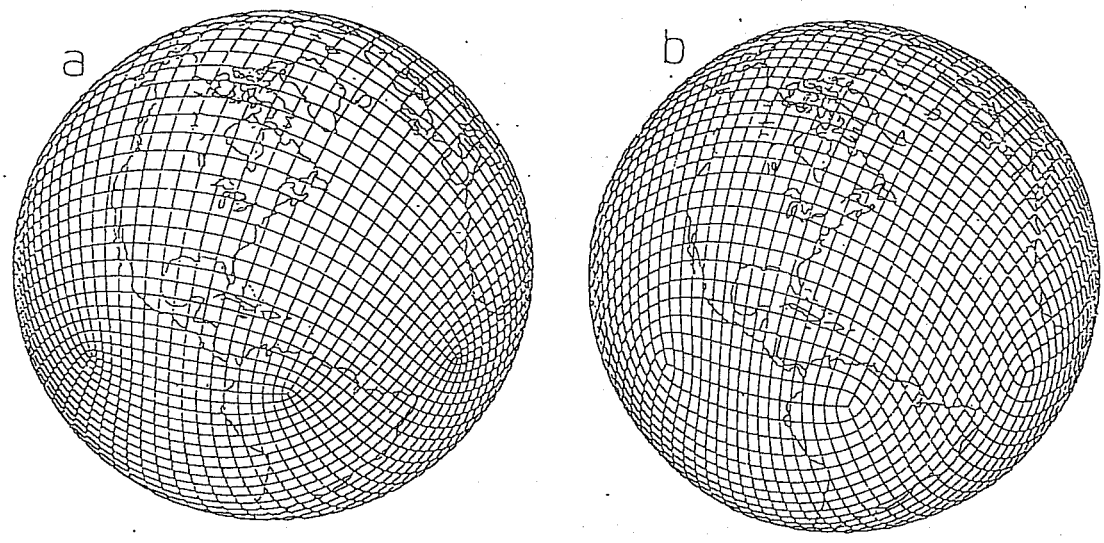

Figure 10. Same as fig. 9, but for the symmetric octagon

The general solution of this problem does not lend itself to such elegant complex-analytic procedures as the examples of conformal mappings do. Solutions have been found using an iterative multigrid method applied to a very fine grid, from which the required model grid is interpolated.

Figs 10a and 10b show the corresponding grids for a conformal and "smoothed" symmetric octagon with vertices placed around the equator. The experiments of Purser and Rančić (1998) show some evidence that a more homogeneously resolving smooth grid could be beneficial, in spite of the loss of grid orthogonality incurred. These experiments indicate a slight advantage in favour of the the cubic arrangement over the octagonal for global modelling (Dr. John McGregor [personal communication] reports a similar finding for the case of his semi-Lagrangian model [McGregor, 1996] applied to these

grid geometries). However, one application where the octagonal arrangement has the advantage is in the case of an autonomous model, of global extent, but distorted smoothly to provide enhanced resolution in one (approximately circular) geographical region. Of course, this is precisely the aforementioned idea of Schmidt (1977), simply translated to the context of our gridded domains. Purser and Rančić (1997) show that, applying the Schmidt dilatation centrally to a conformal octagon grid gives an effectively circular region, bounded by the eight vertices, in which the enhanced grid resolution obtained is practically uniform (fig. 11). It therefore seems that the octagonal grids are potentially more useful in providing detailed regional simulations than in global modelling. Presumably, the same applies to dodecagonal constructions using triangular grids.

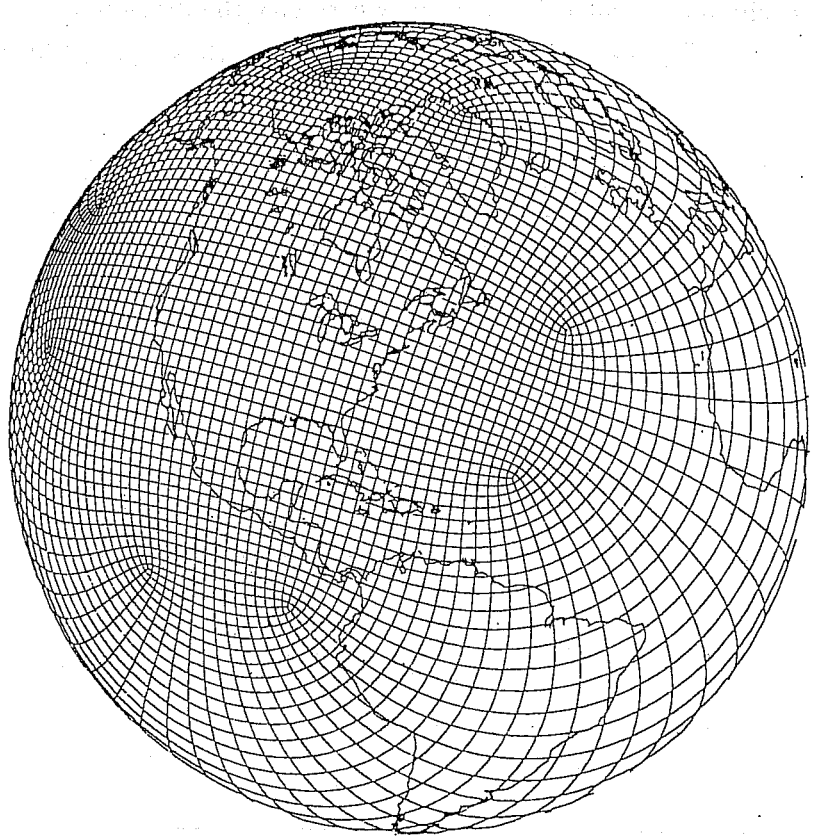

Figure 11. Conformal octagon with regionally enhanced resolution

3.5 Quasi-regular gridded octagons and dodecagons.

For both the square-gridded octagon and the triangular-gridded dodecagon, there is an elegent way to select the relative dimensions of the alternating sides in order to produce the shape which, for its overall resolution, best approximates the corresponding regular polygon. First consider the case of the octagon and suppose successives sides, in grid units, are a and b, where a is an integer but b is some integer times $\sqrt{2}$. The diameters parallel to these sides are then, respectively, $a + \sqrt{2}b$ and $b + \sqrt{2}a$, which are more nearly "equal" than are the original sides. This suggests an obvious recursive procedure, generating successively more regular gridded octagons, starting with the trivial degenerate case, $a_0 = 1$, $b_0 = 0$. Table 1 lists the first few pairs, a and b, derived by this recursion, together with a measure of the departure from regularity. A similar procedure on the triangular grid pertains to the generation of successively more regular dodecagons, where now the diameters associated with sides a and b are, $2a + \sqrt{3}b$, $2b + \sqrt{3}a$, and where b is now some integer times $\sqrt{3}$. Table 2 lists the first few pairs, a and b, in this case.

TABLE 1. RELATIVE LENGTHS OF ALTERNATING SIDES OF A RECURSIVE SEQUENCE OF QUASI-REGULAR SQUARE-GRIDDED OCTAGONS.

k	a_k (sides parallel to grid lines)	b_k (sides 45° to grid lines)	$\epsilon_k = (b_k/a_k - 1)$
0	1	0	-1.0000
1	1	$\sqrt{2}$	.4142
2	3	$2\sqrt{2}$	-.0572
3	7	$5\sqrt{2}$	.0102
4	17	$12\sqrt{2}$	-.0017
5	41	$29\sqrt{2}$	.0003

TABLE 2. RELATIVE LENGTHS OF ALTERNATING SIDES OF A RECURSIVE SEQUENCE OF QUASI-REGULAR TRIANGULAR-GRIDDED DODECAGONS.

k	a_k (sides parallel to grid lines)	b_k (sides 30° to grid lines)	$\epsilon_k = (b_k/a_k - 1)$
0	1	0	-1.000000
1	2	$\sqrt{3}$	-.133975
2	7	$4\sqrt{3}$	-.010257
3	26	$15\sqrt{3}$	-.000740
4	97	$56\sqrt{3}$	-.000053
5	362	$209\sqrt{3}$	-.000004

3.6 Treating the problem of singularities in smooth grids.

McGregor (1996, 1997) has very successfully employed both conformal and (stretched) gnomonic cubic grids for use in a global semi-Lagrangian model. It seems that this approach can also be profitably applied to icosahedral grids (Dr. F. Giraldo, personal communication). Semi-Lagrangian models are

usually less sensitive than Eulerian models to problems in advection associated with grid singularities. But in Eulerian models not possessing customised differencing templates for the problematic areas, the presence of even the weak singularities of the grid coordinate in the otherwise conformal or smoothly quasi-homogeneous grids described in the preceeding subsections remains a significant problem that has hindered the adoption of these grids. The approach of Ronchi et al. (1996) does not suffer this potential defect because the coordinates on which the six grids are based are without singularities at the vertices of the cube. But this approach does not enjoy the virtue of a grid smoothly continuous across the edges of each large square, even away from the vertices. We complete our survey of polyhedron-based grids by discussing a technique by which the conformal mapping geometries may be systematically modified, but only close to each vertex, in such a way that the modified region on each separate face of the parent polyhedron blends smoothly with the unmodified region, and each vertex is rehabilitated as a regular point of each face's grid. Like the grid of Ronchi et al. (1996), one face's grid is no longer continuous with that of its neighbours, but at least the family of grid coordinates transversal to the polyhedron's edge still remains smoothly continuous across that edge.

For a vertex with angular deficiency $90° = 2\pi/4$ we recall that the conformal mapping involved finding a complex analytic function of the form $w(z) = f(\tilde{w})$ for what we here define as $\tilde{w}(z) = z^{4/3}$. If we take real and imaginary components of z to be x and y we find that the images of the coordinate lines of constant x and y mapped into the $\tilde{w}$-plane form "trajectories" obeying "dynamics" with respect to a (real) pseudo-time parameter, t:

$$\frac{d^2\tilde{w}}{dt^2} = \frac{1}{4}\frac{(d\tilde{w}/dt)^2}{\tilde{w}}. \tag{3.10}$$

Similarly, in the triangular grids, for a vertex of angular deficiency $60° = 2\pi/6$ and where the conformal mapping takes the same form, but with $\tilde{w}(z) = z^{6/5}$, the appropriate "dynamics" are given by

$$\frac{d^2\tilde{w}}{dt^2} = \frac{1}{6}\frac{(d\tilde{w}/dt)^2}{\tilde{w}}. \tag{3.11}$$

Now it is easy to appreciate that, if the "force" for these dynamics is smoothly and progressively diluted to zero as $\tilde{w}$ tends to zero, the "trajectories" (grid lines) which were hitherto stongly curved near $z = \tilde{w} = 0$ are replaced by curves which become quite straight near this vertex. As an example, fig. 12 shows the result in the $\tilde{w}$-plane of multiplying the original "forces" of (3.10) and (3.11) by a dilution function,

$$\beta(\tilde{w}/\tilde{w}_*), \tag{3.12}$$

where

$$\beta(s) = \begin{cases} 1 - (1 - |s|^2)^2 & : \quad s < 1 \\ \\ 0 & : \quad s \geq 1 \end{cases} \tag{3.13}$$

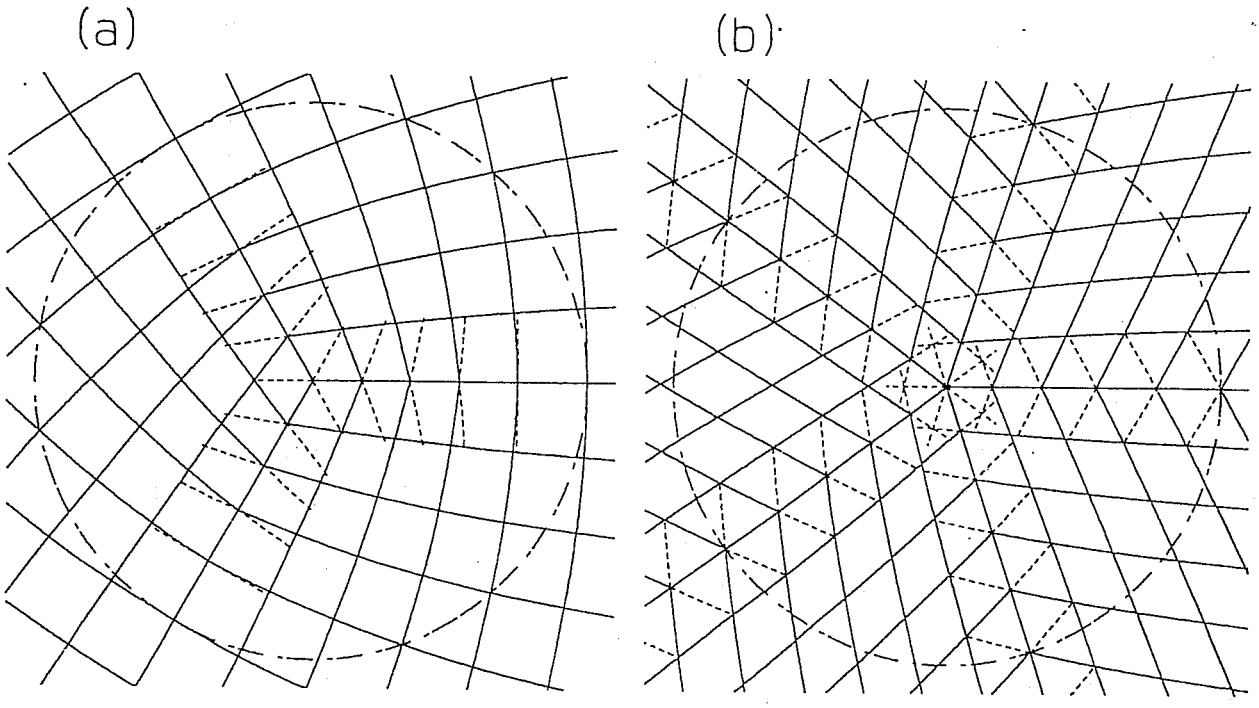

Figure 12. Modified conformal grids in their $\tilde{w}$-planes in the vicinity of a vertex for: (a) three adjoining square grids around a vertex with an angular deficiency of 90°; (b) five adjoining triangular grids around a vertex with an angular deficiency of 60°.

The circles in fig. 12 correspond to $|\tilde{w}| = \tilde{w}_*$, the boundary of the region where dynamics are diluted in this manner. Clearly, it is possible to adopt alternative "dilution functions" to achieve higher degrees of continuity at the bounding circle or at the vertex; the important point to note is that *every* vertex of angular deficiency 90° can have its conformal grid inside the chosen circle (in its $\tilde{w}$-plane) replaced by the diluted-dynamics alternative depicted in fig. 12a. Similarly, for a triangular grid arrangement with vertices of angular deficiency 60°, the appropriate surgery is the replacement, within the chosen circle, of the configuration of fig. 12b.

These patches provides a way of avoiding the principal outstanding problem of the conformal grids, namely, their coordinate singularities, while retaining their desirable feature of smooth continuity along at least the central segment of each polygon-edge. They may also be regarded as a way in which the benefits of the partially continuous grids of Ronchi et al. (1996) may be attained in grids other than the cube and, in particular, in the various triangular grids where, in no case, is there a suitable projective analogue corresponding to the gnomonic projection Ronchi et al. employ.

4. NUMERICAL DIFFERENCING ON TRIANGULAR GRIDS

This section examines some of the special problems that arise in designing numerical differencing templates on triangular/hexagonal grids. We examine only methods which treat the three principal grid orientations on an equal footing.

4.1 Difficulties with staggered grids

Many successful grid point models based on rectangular grid frameworks have used Arakawa-type differencing schemes (e.g., Black 1994), in order to achieve control of the down-scale cascade of energy and enstrophy with minimal additional artificial smoothing. The best such schemes require a staggering of the variables in the horizontal, so it might be reasonable to suppose that corresponding numerical benefits would be gained in the context of triangular grids by staggering the variables. Ničković (1994) investigated the triangular counterpart to the Arakawa "C" grid and, very recently, Ničković and Mesinger (personal communication) have investigated the characteristic properties of all the triangular (or "hexagonal") analogues of the staggered grids classified in Arakawa and Lamb (1977). Figure 13 is a schematic depiction of these grids, which Ničković and Mesinger refer to as

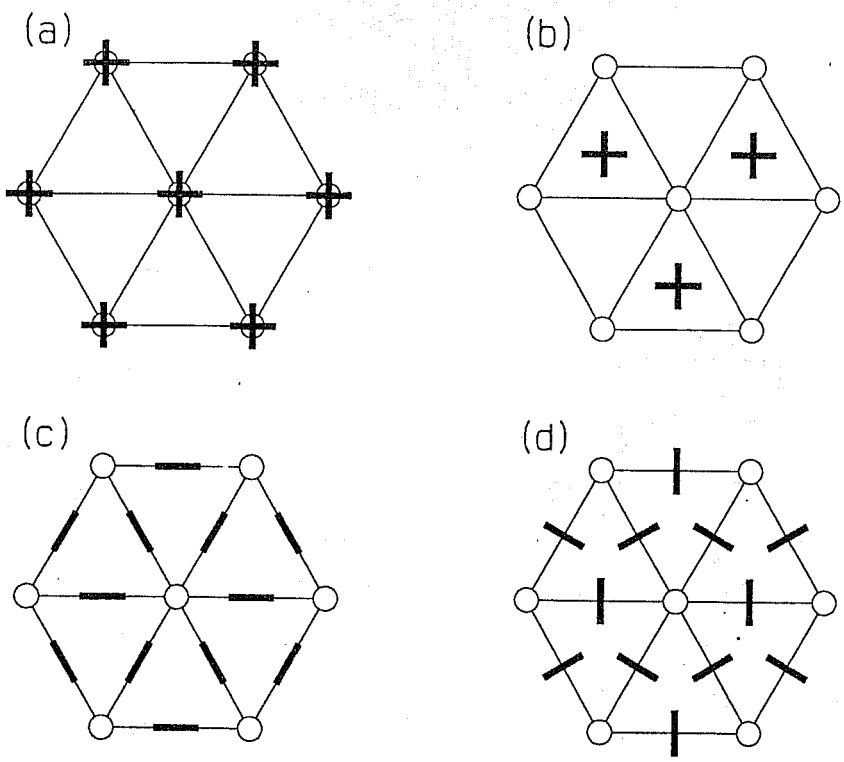

Figure 13. Classification of staggered triangular/hexagonal grids: (a) HA; (b) HB/E; (c) HC; (d) HD. Mass variables reside at circles, wind components at solid bars, in the direction indicated by each bar.

grids HA — HD (for "hexagonal"). The circles mark the locations of the mass points and the thick bars mark the locations and orientations of each grid's wind components. On a flat infinite domain, the wave-vectors, (k, l), resolved by a triangular grid of unit spacing aligned with the conventional

"x" direction are those bounded by a regular hexagon with corners at the point $(k, l) = (4\pi/3, 0)$ and its images under 60° rotations about the origin. It is instructive to examine how the staggered grids treat the linearized non-dimensional f-plane shallow water equations,

$$\frac{\partial u}{\partial t} - v + \frac{\partial \phi}{\partial x} = 0, \tag{4.14}$$

$$\frac{\partial v}{\partial t} + u + \frac{\partial \phi}{\partial y} = 0, \tag{4.15}$$

$$\frac{\partial \phi}{\partial t} + c^2 \left(\frac{\partial u}{\partial x} + \frac{\partial v}{\partial y} \right) = 0, \tag{4.16}$$

where c is a parameter expressing, in grid units, the Rossby radius of deformation.

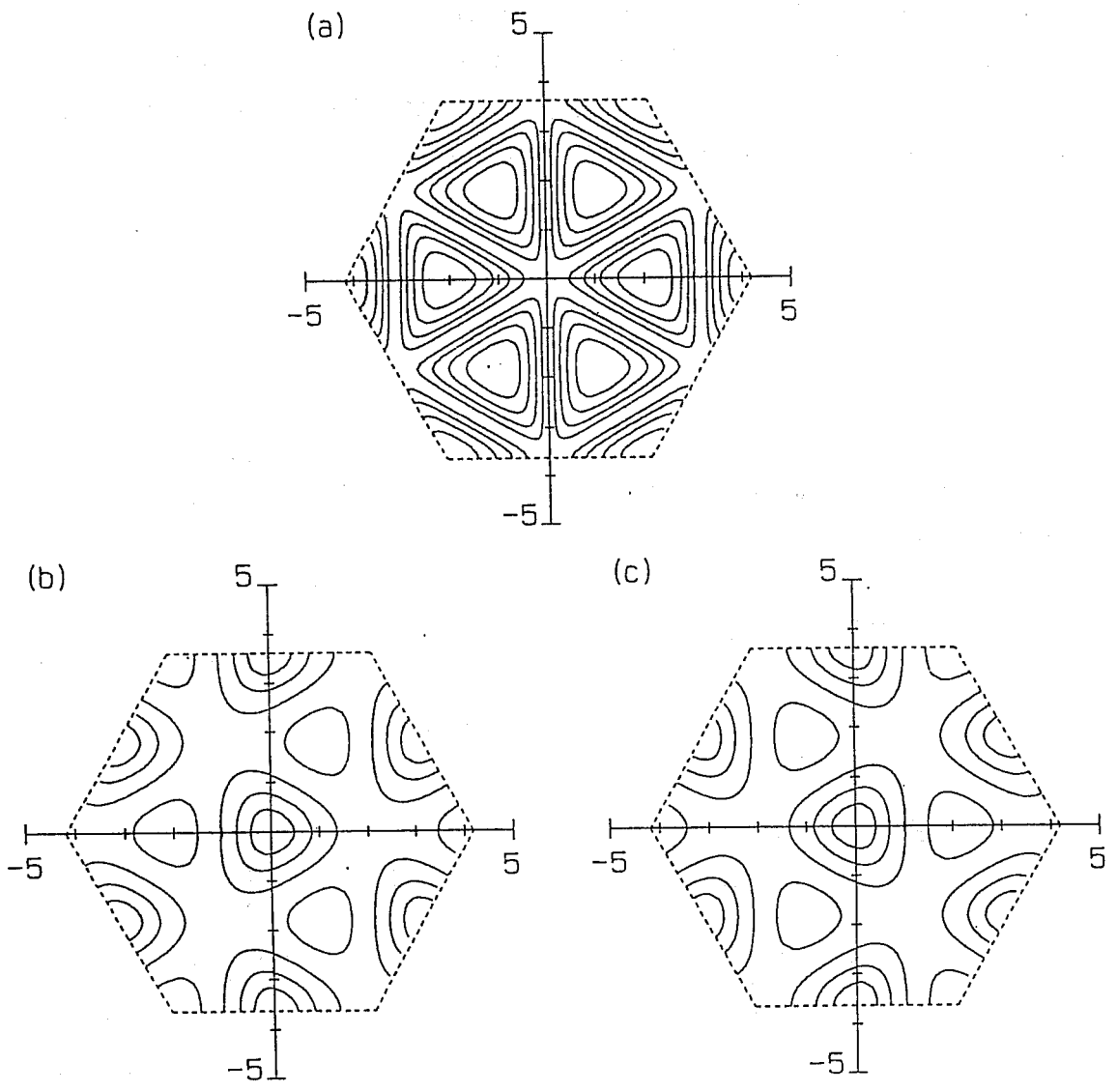

Figure 14. Contours of the magnitudes of frequencies of modes obtained in the grid HB/E, plotted in wave-vector space, for a Rossby radius of 2 grid units. (a) The quasi-geostrophic mode, showing a spuriously nonvanishing frequency (contours in increments of 0.2); (b) and (c) the two components of gravity-inertia waves showing the asymmetry between eastward and westward-propagating components. (Contours of unity, unit frequency for inertial oscillations at the origin.)

For the grid HB/E (defined by fig. 13b) Ničković and Mesinger find that there is an undesirable asymmetry between the speeds of an eastward propagating gravity-inertia wave and its westward-

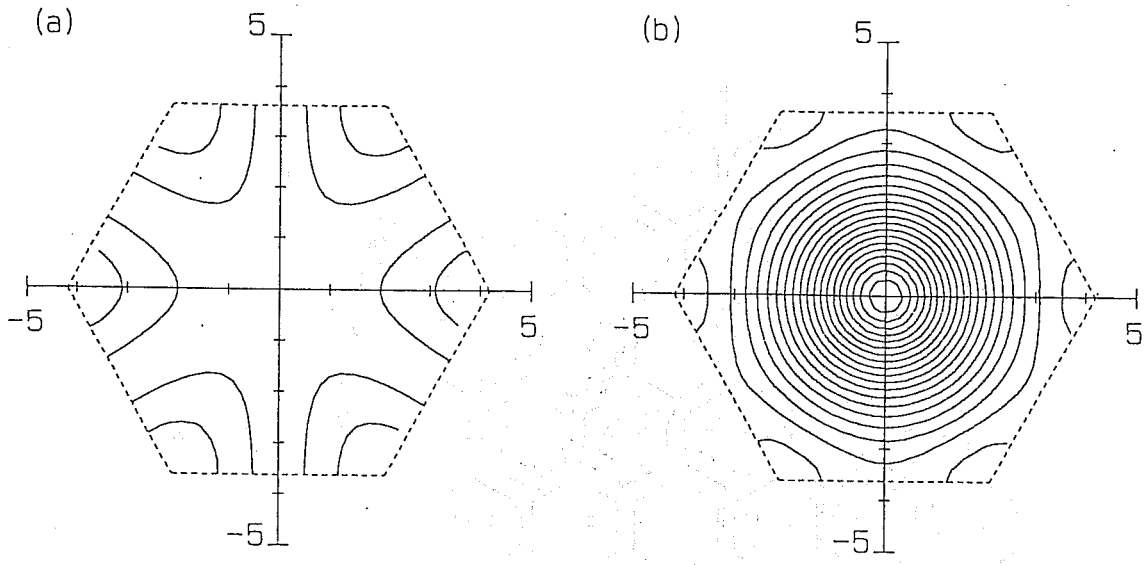

Figure 15. Contours of the magnitudes of frequencies of modes obtained in the grid HC, plotted in wave-vector space, for a Rossby radius of 2 grid units. (a) The quasi-geostrophic mode, showing a spuriously nonvanishing frequency; (b) gravity-inertia waves (contours in increments of 0.2 nondimensional units in both plots.)

propagating mirror-image. The frequencies of these two modes are contoured in the domain of allowed wave-vectors in figs. 14b and 14c for the parameter $c = 2$. A much more serious problem, which unfortuantely affects all of the staggered triangular grids, is that the supposedly stationary quasi-geostrophic mode possesses a non-vanishing frequency at some orientations, and therefore propagates. Fig. 14a shows contours of these spurious frequencies. For the grid HC (defined by the arrangement shown in fig. 13c) the gravity-inertia waves remain symmetrical under mirror-reflection symmetry (fig. 15b) but, instead of a single stationary quasi-geostropic mode, there are now two, and both propagate spuriously (fig. 15a). The HD grid (not shown here) also possesses a pair of spuriously propagating non-stationary quasi-geostrophic modes. It therefore seems that the Arakawa-style numerical schemes with staggered grids are not applicable in any obvious way to a practical meteorological model based on the triangular grid arrangement.

4.2 High-order differencing on a triangular grid.

Instead of applying second-order energy and enstrophy conserving numerics to a staggered grid, an alternative approach to achieving faithful simulations of atmospheric flows is to use high-order numerical methods on the simplest, unstaggered, grid. Here we examine this option for the symmetric triangular grid. We shall employ the indexing convention for differencing templates suggested by fig. 16. Thus, for the two indices, (i, j), the x and y relative displacements implied on a unit-spaced grid are $x = i/2$, $y = j\sqrt{3}/2$. We shall be concerned with derivations of coefficients of the two orthogonal components of the numerical gradient operator that respect the local symmetries of the grid. These symmetries (formally, the "dihedral group of order 12", the symmetries of the regular hexagonal dihedron) comprise the horizontal rotations about the centre by multiples of 60° and mirror-reflections across horizontal axes oriented at multiples of 30°. The sine and cosine of azimuth (relative to the positive x-axis) of a grid displacement indexed (i, j) will be denoted respectively by $S(i, j)$ and

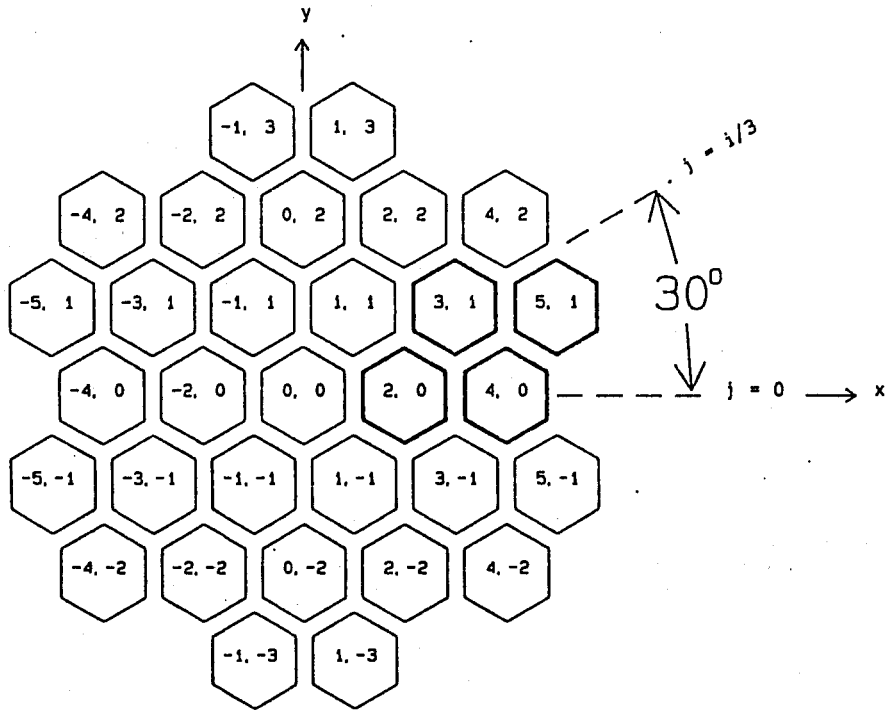

Figure 16. Indexing convention for the template members of a gradient operator on a triangular grid. The coefficients of members of the template X for the x-derivative within the 30° sector (highlighted members) suffice, by symmetry, to determine the remaining X-coefficients and the entire set of Y-coefficients for the y-derivative.

$C(i,j)$ and are defined:

$$S(i,j) = \frac{j\sqrt{3}}{(i^2+3j^2)^{1/2}}, \tag{4.17}$$

$$C(i,j) = \frac{i}{(i^2+3j^2)^{1/2}}. \tag{4.18}$$

We shall write "$(i,j) \equiv (i',j')$" to mean that the relative displacements (i,j) and (i',j') can be brought into equivalence by the application, to one of these grid displacements, of a member of the grid's local symmetry group defined above. If the x- and y-components of the numerical gradient template at (i,j) are denoted by $X_{(i,j)}$ and $Y_{(i,j)}$, then the condition that this gradient operator is faithful to the local grid symmetries is that:

$$C(i',j')X_{(i,j)} = C(i,j)X_{(i',j')}, \tag{4.19}$$

$$S(i',j')X_{(i,j)} = C(i,j)Y_{(i',j')}, \tag{4.20}$$

whenever $(i,j) \equiv (i',j')$. A symmetry-preserving gradient approximation can therefore be defined uniquely by specifying only the coefficients of the $X_{(i,j)}$ components of displacements that belong to the 30° sector, $0 < i$, $0 \leq 3j \leq i$, which is also indicated in fig. 16.

Two examples of such gradient operators are shown in figs. 17 and 18, for the "first quadrant", $x \geq 0$, $y \geq 0$, only. Both are sixth-order schemes, panel (a) shows the coefficients $X_{(i,j)}$, while (b) displays the quantities, $Y_{(i,j)}/\sqrt{3}$ in their proper locations. Thus, contrary to the case of the unstaggered square

TABLE 3. COEFFICIENTS OF RADIAL TEMPLATE HIGH-ORDER GRADIENT OPERATORS FOR TRIANGULAR GRIDS

scheme	R_2	R_4	R_6	R_8	R_{10}	R_{12}	R_{14}	R_{16}
β	3	18	90	1260	3780	41580	540540	1081080
$\beta X_{(2,0)}$	1	8	45	672	2100	23760	315315	640640
$\beta X_{(4,0)}$		-1	-9	-168	-600	-7425	-105105	-224224
$\beta X_{(6,0)}$			1	32	150	2200	35035	81536
$\beta X_{(8,0)}$				-3	-25	-495	-9555	-25480
$\beta X_{(10,0)}$					2	72	1911	6267
$\beta X_{(12,0)}$						-5	-245	-1120
$\beta X_{(14,0)}$							15	128
$\beta X_{(16,0)}$								-7

TABLE 4. COEFFICIENTS OF SOLID TEMPLATE HIGH-ORDER GRADIENT OPERATORS FOR TRIANGULAR GRIDS

scheme	S_2	S_4	S_6	S_8	S_{10}	S_{12}	S_{14}	S_{16}
β	3	12	540	2520	4148000	138600	3052249200	85765680
$\beta X_{(2,0)}$	1	6	304	1560	2844698	93366	2189574240	62520624
$\beta X_{(3,1)}$		-1	-54	-360	-961596	-24885	-759887172	-22101708
$\beta X_{(5,1)}$			5	60	228610	6525	237277515	7590645
$\beta X_{(4,0)}$			-22	-138	-131538	-12348	-206742624	-6758262
$\beta X_{(6,2)}$				-9	-106749	-1710	-117694908	-4225966
$\beta X_{(6,0)}$				-8	-155418	-102	-112093206	-3483494
$\beta X_{(8,2)}$					1760	216	15677528	755400
$\beta X_{(7,1)}$					52227	-630	18859015	585963
$\beta X_{(8,0)}$					-16022	234	12469844	579942
$\beta X_{(9,3)}$						-25	-4152242	-345686
$\beta X_{(9,1)}$						-27	-12205539	-678597
$\beta X_{(11,3)}$							66550	8976
$\beta X_{(10,2)}$							1609170	179385
$\beta X_{(11,1)}$							-500753	-82071
$\beta X_{(10,0)}$							5210810	382842
$\beta X_{(12,4)}$								-833
$\beta X_{(12,2)}$								-1088
$\beta X_{(12,0)}$								15874

grid, where there is essentially only one obvious candidate for explicit numerical gradient operator at a given order of accuracy, in the case of the triangular grid we are generally faced with some choice. Fig. 17 exhibits the sixth-order member, R_6, of what we might refer to as the "radial template" family of high-order gradient operators; these are just the symmetry-respecting adaptations of the standard one-dimensional high-order differencing operators, applied with appropriate weights along the three principal lines of the triangular grid. The coefficients for these schemes up to 16th order are given in table 3.

Fig. 18 exhibits the sixth-order member, S_6, of what we shall refer to here as the "solid tem-

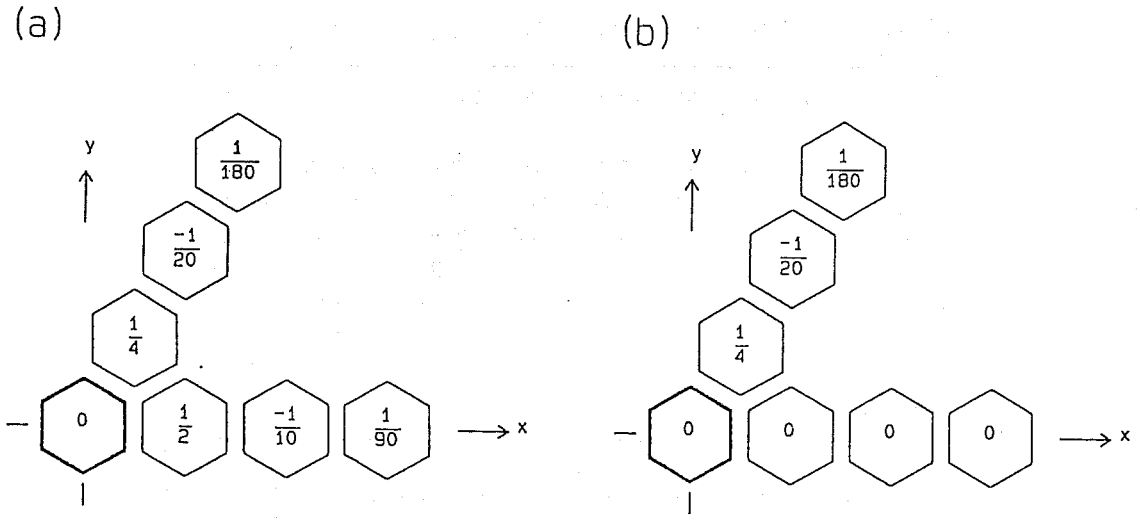

Figure 17. The first quadrant of the sixth-order "radial template" gradient operator, R_6; (a) components, $X_{(i,j)}$ for x-derivatives; (b) components, $Y_{(i,j)}/\sqrt{3}$ for y-derivatives

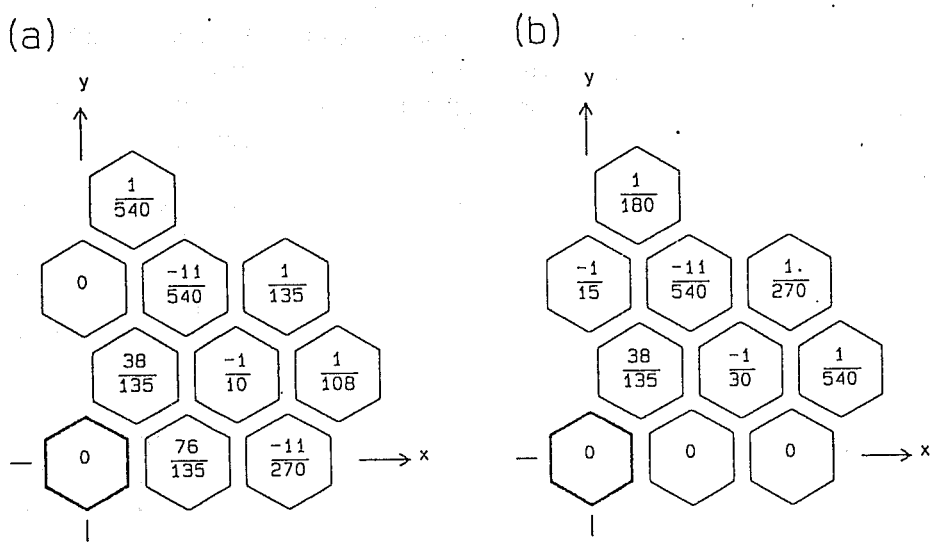

Figure 18. The first quadrant of sixth-order "solid-template" gradient operator, S_6; (a) coefficients, $X_{(i,j)}$; (b) coefficients, $Y_{(i,j)}/\sqrt{3}$.

plate" family. Each member, S_N, of this family is defined to be the "best" (in the sense we explain below) symmetry-respecting scheme whose template of relative displacements (i, j) from the point of evaluation fits within the hexagonal region for which $j' \leq (2 + 3N)/8$ for each $(i', j') \equiv (i, j)$. Let us consider how we might objectively rank alternative differencing schemes in a way consistent with the notion that a high-order scheme is better than one of lower order. Recall that a gradient scheme of order N evaluates *exactly* the derivative components of any spatial distribution consisting of a polynomial of degree-N jointly in x and y. This implies that, applied to unit-amplitude Fourier waves, $\exp(i[kx + ly])$, the error, numerical-minus-true, is a function of k and l whose Taylor-series coefficients vanish for powers of k and l jointly not exceeding N. Suppose we add together the squares of the

absolute magnitudes of the x and y components of the gradient error at each (k, l) and integrate this quantity with respect to azimuth around each circle of constant $K = (k^2 + l^2)^{1/2}$, thereby obtaining a radial error function $\varepsilon(K)$ of the total wavenumber. This is an even function of K possessing an expansion about the origin:

$$\varepsilon(K) = \varepsilon_0 + \varepsilon_2 K^2 \ldots \tag{4.21}$$

for which all coefficients, ε_{2p}, for $p \leq N$ vanish in a gradient scheme of order N. However, this suggests a procedure for ranking competing differencing schemes and achieving a definite verdict even when their formal orders of accuracy are the same. We do this by means of a progressive comparison of the magnitudes of these expansion coefficients, and favour scheme "A" over scheme "B" when it is found, for some index q, that $\varepsilon_p^{(A)} = \varepsilon_p^{(B)}$ for all $p < q$, but $\varepsilon_q^{(A)} < \varepsilon_q^{(B)}$. The ε_p are quadratic functions jointly of the independent template coefficients, $X_{(i,j)}$, of the gradient scheme, so the constrained minimization problem of determining the "best" scheme for a given template becomes a linear one and, since the functional relationships involve only rational coefficients, the solutions are guaranteed to produce template coefficients which are also expressible in terms of rationals. The first few of the schemes S_N have been determined by this procedure and their representative coefficients $X_{(i,j)}$ in the principal 30° sector are listed in table 4.

The reason we might wish to consider the more compact schemes S_N in preference to the equivalent order schemes R_N is revealed in fig. 19, which plots the absolute magnitudes of the truncations errors of the two schemes S_{12} (fig. 19a) and R_{12} (fig. 19b), normalized by the absolute magnitudes, at each wave-vector, of the true gradient. As we have already seen, the triangular grid is theoretically capable of resolving Fourier waves of wavenumbers exceeding (by up to 1/3) the "Nyquist" sampling frequency limit of a single grid line. However, the simple-minded application of one-dimensional high-order differencing schemes to this grid, forming the family of schemes R_N, does *not* fully exploit this range of wavevectors. In effect, these radial template schemes are degrading the resolution. The alternative schemes, S_N, *do* exploit the triangular grid's resolution to the full, but would be costly to apply at high-order in the most straight-forward way.

There is one way in which high-order solid template schemes might be made practically viable without disproportionate computational cost; by performing the convolutions they imply indirectly, on the Fourier-transformed data. Since the templates possess compact support the influence of their convolutions is limited to a finite radius. This means that the artificial imposition of periodicity on a large enough rectangular or hexagonal subdomain of a more extensive grid will not spoil the interior result. Overlapping subdomains, suitably chosen, can then cover all parts of a global grid except where singularities intrude and break the symmetry.

4.3 High-order differencing where the grid is irregular.

If the singularities cannot be deferred, beyond the edges of each large face of a polyhedral grid, as occurs in the modified conformal grids of subsection (3.6), then, at these points and regardless of the manner in which the high-order differencing is implemented, it becomes necessary to revert to customised numerical differencing templates for each individual point in the halo of influence of the

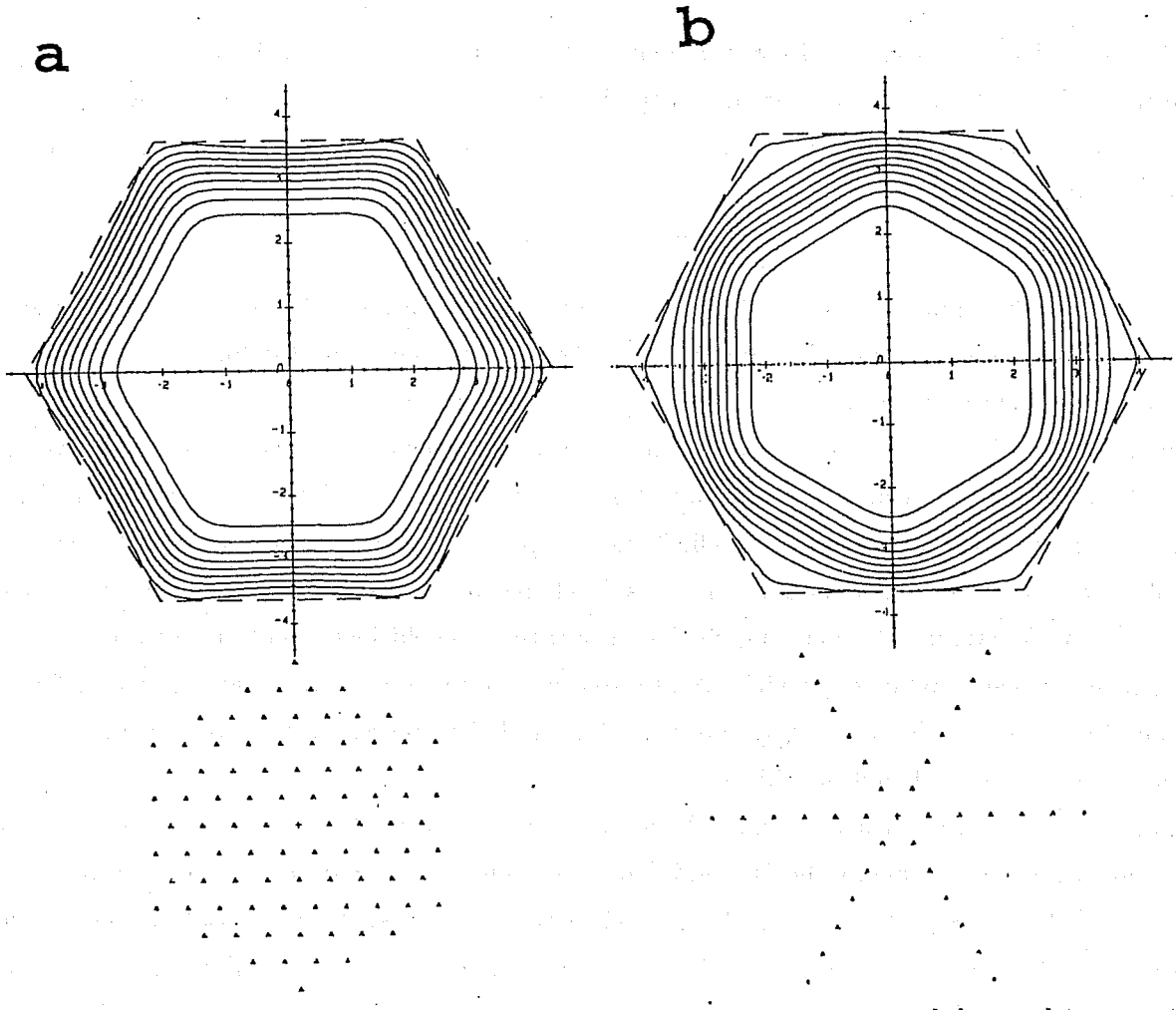

Figure 19. Normalized magnitude of truncation error contoured in wave-vector space, and the template supports, for 12th-order gradient schemes: (a) S_{12}; (b) R_{12}; suggesting the inability of the latter family of schemes to match the theoretical resolution the triangular grid allows.

offending grid singularity. We shall therefore complete this section with a brief sketch of a method of template construction proposed by Swartztrauber et al. (1997) for icosahedral/triangular grids not necessarily possessing the exact symmetries we have been assuming throughout the earlier part of this section.

Essentially, their technique is to apply a least-squares variant of the collocation method. They find spatial differencing coefficients which are exact for the most important "smoothest" test functions (a strongly enforced set of linear constraints) while, for a remaining set of slightly less critical test functions, the overall squared error norms are minimised, subject to the aforementioned strong constraints. Since they are concerned with spherical geometry, they use test functions comprising the spherical harmonics of lowest total degree; these are, in one sense, the analogues on the sphere of the Fourier plane waves, but, in another sense which their method exploits, they can also be regarded as disguised polynomials of the three earth-centred cartesian coordinates. One potential problem in the general case of unstructured clusters of grid points is the numerical ill-conditioning of the constrained error-minimisation; their suggestion is to use the method of singular value decomposition (e.g., Golub and Van Loan, 1989), which is a tool both for inspecting the conditioning characteristics, and for carrying out the actual minimisations in a numerically well-behaved way.

In the planar version of this technique, the test functions would be the special polynomials in $x = r\cos\theta$ and $y = r\sin\theta$ possessing either of the forms,

$$P_{n,m}(x,y) = r^n \cos(m\theta), \tag{4.22}$$

$$Q_{n,m}(x,y) = r^n \sin(m\theta), \tag{4.23}$$

where n is the total degree, $m \leq n$ is the azimuthal wavenumber and $n - m$ is even. It is possible to show that the principles we stated for defining the "best" solid-template gradient schemes of section 4.2 lead naturally to an exactly equivalent least-squares collocation method using these test functions. For regions of a triangular grid, such as near the vertices of the spherical icosahedron, where the local regularity of the grid is disrupted, the application of the planar adaptation of the method of Swarztrauber et al. to a smooth map projection (such as is provided by the "$\tilde{w}$-plane of the conformal-icosahedral mapping) of the relevant cluster of grid points, might actually prove to be a simpler alternative for the generation of the customised differencing templates than applying the original spherical-harmonic version of their method to the true grid point locations on the spherical surface. In any event, the conditional least-squares collocation method provides a systematic way of directly addressing the problem of achieving high-order accuracy within the halo of influence of a singularity which, in contrast to the method suggested in section 3.6, does *not* require any surgical modification of the grid itself.

5. DISCUSSION

We have considered several non-standard grid arrangements for the spherical domain, based on mapping the surfaces of polyhedra (possibly of the degenerate, flat, kind) and discussed the virtues and vices intrinsic to these configurations. For three-dimensional Eulerian models, the continued presence of grid-singularities (at the images of the vertices) within otherwise smooth grids constructed by either conformal or variational procedures causes residual spurious numerical artifacts (possibly related to the resonant forcing of quasi-stationary internal gravity modes) to appear there in many models. The singularities do not seem to cause significant problems in a semi-Lagrangian treatment (McGregor 1996) and, in high-order Eulerian models, the problem of singularities can be ameliorated by devising special differencing templates near each vertex and, in the construction of the differencing schemes there, regarding the spatial distribution of grid points as unstructured (Swarztrauber et al., 1997). The excellent results achieved by Ronchi et al. (1996) suggest that it is preferable to use several regionally-smooth grids, each remaining well-behaved up to and beyond any vertex, rather than using a single grid system (such as the unmodified global conformal grids) in which singularities in the grid coordinate metrics cannot be avoided. With this principle in view, we have indicated in section (3.6) how any conformal grid may be surgically altered to recover the desirable generic properties first exhibited, for the particular case of the cube, by the grid of Ronchi et al. (1995).

The higher local symmetry of the triangular grid (compared to the square grid) makes it immediately attractive as a framework for dynamically modelling the atmosphere, especially on the global domain where the icosahedral grid boasts such an exceptionally uniform resolution. In some applications,

where "physics" within the vertical columns or chemical interactions at individual points, overwhelmingly dominate the computational demands made by the model, some form of the icosahedral grid arrangement must always be considered one of the strongest candidates, owing to this configuration's inherent ability to allocate horizontal area equitably among the vertical columns. However, as we have seen, the triangular arrangement for horizontal differencing conceals several subtle difficulties. There is, as yet, no obvious way in which the energy- and enstrophy-conserving style of staggered grid schemes can be applied to the triangular grid without incurring such anomalies as asymmetrical gravity wave propagation and non-steady (quasi-)geostrophic modes (Ničković and Mesinger, personal communication). Even on the unstaggered grid, where one might hope to gain an advantage through the use of high-order differencing schemes, we find that the simplest gradient operators ("radial template" schemes in our terminology), which are already more costly to apply than their square-grid counterparts, are actually inadequate in utilising the resolution that the triangular grid is theoretically capable of. And the more complicated "solid template" schemes, which *do* properly use the grid's full resolving capability, are considerably more costly to apply. These are features of the triangular grid that deserve careful quantitative examination before a serious commitment to such a grid is made. Nevertheless, the recent resurgence of serious interest and effort relating to icosahedral grids, exemplified by the recent investigations of Baumgardner and Frederickson (1985), Heikes and Randall (1995a), Giraldo (1997), Steppeler and Majewski (see D. Majewski, these seminars), and the suitability of polyhedral grid framework in general to efficient implementation on MPPs, assures these methods a significant, if specialised, future role.

Acknowledgements

I wish to express my gratitude for the help I received from several colleagues during the preparation of this seminar. In particular, to Profs. S. Ničković and Fedor Mesinger, who very kindly allowed me a preview of their researches, discussed in section 4.1; to Dr. John McGregor (CSIRO, Australia), for his appraisal of the relative quality of various square-grid arrangements used in his semi-Lagrangian model; to Dr Frank Giraldo (NRL, Monterey), for sharing material relating to his use of icosahedral grids; finally, to Dr. M. Rančić (NAS/GSFC), who first stimulated my interest in this topic and who provided many valuable insights into strengths and weaknesses of the various possibilities that non-standard gridding allows.

References

Arakawa, A., and V. R. Lamb, 1977: Computational design of the basic dynamical processes of the UCLA general circulation model. *Methods in Computational Physics*, Vol. 17, Academic Press, pp 173–265.

Baumgardner, J. R., and P. O. Frederickson, 1985: Icosahedral discretization of the two-sphere. *SIAM J. Numer. Anal.*, **22**, 1107–1115.

Black, T. L., 1994: The new NMC mesoscale Eta model: Description and forecast examples. *Wea. Forecasting,* **9**, 265–278.

Courtier, P., and J.-F. Geleyn, 1988: A global numerical weather prediction model with variable resolution: Application to the shallow-water equations. *Quart. J. Roy. Meteor. Soc.*, **114**, 1321–1346.

Coxeter, H. S. M., 1973: *Regular polytopes.* Dover, New York. 321pp.

Cullen, M. J. P., 1974: Integrations of the primitive equations on a sphere using the finite-element method. *Q. J. R. Meteorol. Soc.*, **100**, 555–562.

Gates, W. L., and C. A. Riegel, 1962: A study of numerical errors in the integration of barotropic flows on a spherical grid. *J. Geophys. Res.*, **67**, 773–784.

Giraldo, F. X., 1997: Lagrange-Galerkin methods on spherical geodesic grids. *J. Comput. Phys.*, **136**, 197–213.

Golub, G. H., and C. F. Van Loan, 1989: *Matrix computations (Second edition).* Johns Hopkins, Baltimore. 642pp.

Heikes, R., and D. A. Randall, 1995a: Numerical integration of the shallow-water equations on a twisted icosahedral grid. Part I: Basic design and results of tests. *Mon. Wea. Rev.*, **123**, 1862–1880.

Heikes, R., and D. A. Randall, 1995b: Numerical integration of the shallow-water equations on a twisted icosahedral grid. Part II: A detailed description of the grid and an analysis of numerical accuracy. *Mon. Wea. Rev.*, **123**, 1881–1887.

Kurihara, Y., 1965: Numerical integration of the primitive equations on a spherical grid. *Mon. Wea. Rev.*, **93**, 399–415.

Masuda, Y., and H. Ohnishi, 1987: An integration scheme of the primitive equation model with an icosahedral-hexagonal grid system and its application to the shallow water equations. In: *Proceeding of Short- and Medium-Range Numerical Weather Prediction.* T. Matsuno, ed., Meteorological Society of Japan, pp. 317–326.

McGregor, J. L., 1996: Semi-Lagrangian advection on conformal-cubic grids. *Mon. Wea. Rev.*, **124**, 1311–1322.

McGregor, J. L., 1997: Semi-Lagrangian advection on a cubic gnomonic projection of the sphere. In: *Numerical methods in atmospheric and oceanic modelling.* Eds. C. Lin, R. Laprise and H. Ritchie. Canadian Meteorological and Oceanic Soc./NRC Research Press, pp 153–169.

Ničković, S., 1994: On the use of hexagonal grids for simulation of atmospheric processes. *Beitr. Phys. Atmos.*, **67**, 103–107.

Purser, R. J., and Rančić, M., 1997: Conformal octagon: an attractive framework for global models offering quasi-uniform regional enhancement of resolution. *Meteor. Atmos. Phys.*, **62**, 32–48.

Purser, R. J., and Rančić, M., 1998: Smooth quasi-homogeneous gridding of the sphere. *Quart. J. Meteor. Soc.*, **124**, 637–647.

Rančić , M., Purser, R. J. and Mesinger, F., 1996: A global shallow-water model using an expanded spherical cube: Gnomonic versus conformal coordinates. *Quart. J. Roy. Meteor. Soc.*, **122**, 959–982.

Ronchi, C., R. Iacono, and R. S. Paulucci, 1995: Finite difference approximations to the shallow-water equations on a quasi-uniform spherical grid. In *High-performance computers and networking.* Eds. B. Hertzburger and G. Serazzi. Lecture notes in computer science 919. Springer.

Ronchi, C., Iacono, R. and Paolucci, P. S., 1996: The 'cubed sphere': A new method for the solution of partial differential equations in spherical geometry. *J. Comp. Phys.*, **124**, 93–114.

Sadourny, R., 1972: Conservative finite-differencing approximations of the primitive equations on quasi-uniform spherical grids. *Mon. Wea. Rev.*, **100**, 136–144.

Sadourny, R., Arakawa, A. and Mintz, Y., 1968: Integration of the nondivergent barotropic vorticity equation with an icosahedral-hexagonal grid for the sphere. *Mon. Wea. Rev.*, **96**, 351–356.

Schmidt, F., 1977: Variable fine mesh in spectral global models. *Contrib. Atmos. Phys.*, **50**, 211–217.

Schwerdtfeger, H., 1979: *Geometry of complex numbers*, Dover, New York, 200pp.

Swarztrauber, P. N., D. L. Williamson, and J. B. Drake, 1997: The cartesian method for solving partial differential equations in spherical geometry. *Dyn. Atmos. Ocean*, **27**, 679–706.

Thompson, J. F., Warsi, Z. U. A. and Mastin, C. W., 1985: *Numerical Grid Generation: Foundations and Applications*, North-Holland, New York.

Williamson, D. L., 1968: Integration of the barotropic vorticity equation on a spherical geodesic grid. *Tellus*, **20**, 642–653.

Williamson, D. L., 1970: Integration of the primitive barotropic model over a spherical geodesic grid. *Mon. Wea. Rev.*, **98**, 512–520.